

1 **Observing Low Altitude Features in Ozone Concentrations in a**
2 **Shoreline Environment via Uncrewed Aircraft Systems**

3 Josie K. Radtke¹,
4 Benjamin N. Kies¹,
5 Whitney A. Mottishaw¹,
6 Sydney M. Zeuli¹,
7 Aidan T.H. Voon¹,
8 Kelly L. Koerber¹,
9 Grant W. Petty²,
10 Michael P. Vermeuel^{3†},
11 Timothy H. Bertram³,
12 Ankur R. Desai²,
13 Joseph P. Hupy⁴,
14 R. Bradley Pierce^{2,5},
15 Timothy J. Wagner⁵,
16 Patricia A. Cleary¹

17 ¹Department of Chemistry, University of Wisconsin-Eau Claire, 105 Garfield Ave, Eau Claire, WI, USA

18
19 ²Department of Atmospheric and Oceanic Sciences, University of Wisconsin-Madison, 1225 W Dayton St, Madison, WI, USA

20
21 ³Department of Chemistry, University of Wisconsin-Madison, 500 Lincoln Dr, Madison, WI, USA

22
23 ⁴Aviation and Transportation Technology, Purdue Polytechnic Institute, Purdue University, West Lafayette, IN, USA

24
25 ⁵Space Sciences and Engineering Center, University of Wisconsin-Madison, Madison WI, USA

26
27 [†]Now at Department of Soil, Water, and Climate, University of Minnesota, St. Paul, MN, USA

28
29 *Correspondence to:* Patricia A. Cleary (clearypa@uwec.edu)

30

31 **Abstract.** Ozone is a pollutant formed in the atmosphere by photochemical processes involving nitrogen oxides (NO_x) and
32 volatile organic compounds (VOCs) when exposed to sunlight. Tropospheric boundary layer ozone is regularly measured at
33 ground stations and sampled infrequently through balloon, lidar, and crewed aircraft platforms, which have demonstrated
34 characteristic patterns with altitude. Here, to better resolve vertical profiles of ozone within the atmospheric boundary layer,
35 we developed and evaluated an uncrewed aircraft system (UAS) platform for measuring ozone and meteorological parameters
36 of temperature, pressure, and humidity. To evaluate this approach, an UAS was flown with a portable ozone monitor and a
37 meteorological temperature and humidity sensor to compare to tall tower measurements in northern Wisconsin. In June 2020,
38 as a part of the WiscoDISCO20 campaign, a DJI M600 hexacopter UAS was flown with the same sensors to measure Lake
39 Michigan shoreline ozone concentrations. This latter UAS experiment revealed low-altitude structure in ozone concentrations
40 in a shoreline environment showing highest ozone at altitudes from 20-100 mAGL. These first such measurements of low-
41 altitude ozone via UAS in the Great Lakes Region revealed a very shallow layer of ozone rich air lying above the surface.
42

43 **1 Introduction**

44 Ozone at elevated concentrations near the surface is a pollutant that causes respiratory irritation in humans (Bell et al., 2006;
45 Brauner et al., 2016) and oxidative stress on photosynthesizing organisms in many ecosystems (Fuhrer, 2002). In the
46 troposphere, ozone is generated by reactions of nitrogen oxides ($\text{NO}_x = \text{NO} + \text{NO}_2$) and volatile organic compounds (VOCs)
47 exposed to sunlight (Sillman, 1999). NO_x compounds are emitted from combustion sources and VOCs are emitted by biogenic
48 processes and anthropogenic industrial sources such as transportation and evaporated solvents (benzene, formaldehyde, ethyl
49 alcohol, etc.). While ozone is monitored at the surface to meet various air quality monitoring standards, or to understand ozone
50 depositional losses, ozone gradients aloft have been measured in various ways over the years using sondes that reach the
51 stratosphere (Beekmann et al., 1995; Witte et al., 2018), instrumented towers (Crawford et al., 1996; Desjardins et al., 1995),
52 tethered balloons (Chandrasekar et al., 2003; Li et al., 2018; Mazzuca et al., 2017; Zhang et al., 2019; Tang et al., 2021;
53 Demuer et al., 1997; Greenberg et al., 2009; Knapp et al., 1998), and crewed aircraft (e.g. (Kaser et al., 2017; Crawford et al.,
54 1996; Tanimoto et al., 2015; Tarasick et al., 2019; Desjardins et al., 1995). Because ozone is generated by chemical reactions,
55 the confinement of primary pollutants near the surface via atmospheric inversions tends to produce higher ozone concentration
56 events at the surface. Understanding the volume of air in and above an inversion at a shoreline location prone to high ozone
57 events can help elucidate the chemical evolution processes in this environment (Chai et al., 2013; Tang et al., 2021; Tang et
58 al., 2009).

59 Recently there have been an expansion of efforts for Uncrewed Aircraft Systems (UAS) to be used for atmospheric profiling
60 (Telg et al., 2017; Chilson et al., 2019; De Boer et al., 2021; Hemingway et al., 2017; Jacob et al., 2018; Koch et al., 2018;
61 Wainwright et al., 2015; Li et al., 2018). Tethered balloons have been used to study vertical ozone (Demuer et al., 1997; Peng
62 et al., 2008; Knapp et al., 1998; Zhang et al., 2019; Greenberg et al., 2009), and meteorological conditions (Chandrasekar et

63 al., 2003) gathering data at heights ranging from ground level to 1500 meters above ground level, which included evaluations
64 of episodes of biomass burning (Xu et al., 2018) and mesoscale modeling of ozone in the upper troposphere (Peng et al., 2008).
65 UAS platforms measuring atmospheric properties have deployed at heights ranging from ground level to 4000 meters above
66 ground level (Adkins and Sescu, 2017; Chilson et al., 2019; Cook et al., 2013; Greatwood et al., 2017; Hemingway et al.,
67 2017). The portable Personal Ozone Monitor (2B Tech POM) mounted on a UAS performed consistently in comparison to a
68 larger ozone photoanalyzer equipped to a tethered airship in the lower troposphere (Li et al., 2018) but with some significant
69 discrepancies between platforms within the planetary boundary layer. Through modeling efforts using Generalized Additive
70 Models (GAMs) Li et al. (2018) attributed these discrepancies to horizontal separation of platforms and vertical variations in
71 atmospheric structure including temperature and relative humidity.

72 The effect of lake breeze or sea breeze on regional ozone in shoreline environments has been a point of interest in several
73 studies. The association of sea breezes and lake breezes with elevated ozone at shoreline locations have been documented in
74 Houston (Banta et al., 2005), Toronto (Levy et al., 2010; Sills et al., 2011), New York City during LISTOS (Zhang et al.,
75 2020), and near Chesapeake Bay (Gronoff et al., 2019), but few studies have explored vertical profiles within the marine layer
76 structure. The lake and sea breeze meteorology develop from colder air parcels moving over land underneath buoyant warmer
77 air which can create capping inversion which can trap pollutants (Lu and Turco, 1994; Gaza, 1998; Levy et al., 2010; Sills et
78 al., 2011). Multiple groups have found there to be a notable difference in ozone levels during a sea or lake breeze including
79 OWLETS (The Ozone Water-Land Transition Study) in the Chesapeake Bay region (Sullivan et al., 2019), ABLE (Amazon
80 Boundary Layer Experiment) over Manaus Brazil (Guimaras et al., 2020), and a research team in the Salt Lake City region
81 (Blaylock et al., 2017). OWLETS analyzed ozone pollution using ozone sensors mounted onto ships and UAS. These
82 measurements showed that ozone builds up over the bay due to the effect of sea breeze up to 2000 m above sea level (Sullivan
83 et al., 2019). With these observations, Sullivan et al. (2019) attempted to forecast chemical emissions based upon emissions
84 from ships and other emission sources in the bay. During ABLE, Guimaras et al. (2020) used UAS to study the urban nighttime
85 boundary layer over Manaus, Brazil in both the dry and wet seasons. They conducted flights from the center of the city from
86 ground level up to 500 m to quantify the effect humidity has on ozone pollution over Manaus at night (Guimaras et al., 2020).
87 Crewed aircraft were used over the Great Salt Lake in Utah to study ozone levels up to 4000 m above ground level and
88 demonstrated complicating factor of lake breeze transporting contrasting air masses into the region (Blaylock et al., 2017;
89 Crosman et al., 2017; Horel et al., 2016).

90 The relationship between ambient ozone and coastal environments has been investigated by aircraft, mobile platforms for
91 the 2017 Lake Michigan Ozone Study (LMOS) (Cleary et al., 2022b; Doak et al., 2021; Stanier et al., 2021) and UAS for the
92 OWLETS campaign (Gronoff et al., 2019) and multi-UAS strategies for WiscoDISCO-21 (Tirado et al., 2023; Cleary et al.,
93 2022a). Ozone concentrations have been shown to vary with altitude sharply in low-altitude crewed aircraft flights over Lake
94 Michigan (Cleary et al., 2022b; Stanier et al., 2021). During the OWLETS campaign, the high-over-water ozone was
95 investigated by UAS and ship-based platforms, including low ozone titration events. In these transitional environments, model
96 and observation agreement can be improved with the capture of small gradients and modelling marine inversions over water

97 (Abdi-Oskouei et al., 2020; McNider et al., 2018; Cleary et al., 2015). Recent observations over riverine environments have
98 demonstrated the viability of UAS for detecting low altitude variations in ozone and plume chemistry (Li et al., 2021; Guimaras
99 et al., 2020; Ye et al., 2022). The horizontal extent of lake breeze has also been documented at the shoreline to Lake Michigan
100 where horizontal gradients close to the shoreline were observed during 2017 LMOS (Cleary et al., 2022b; Stanier et al., 2021).

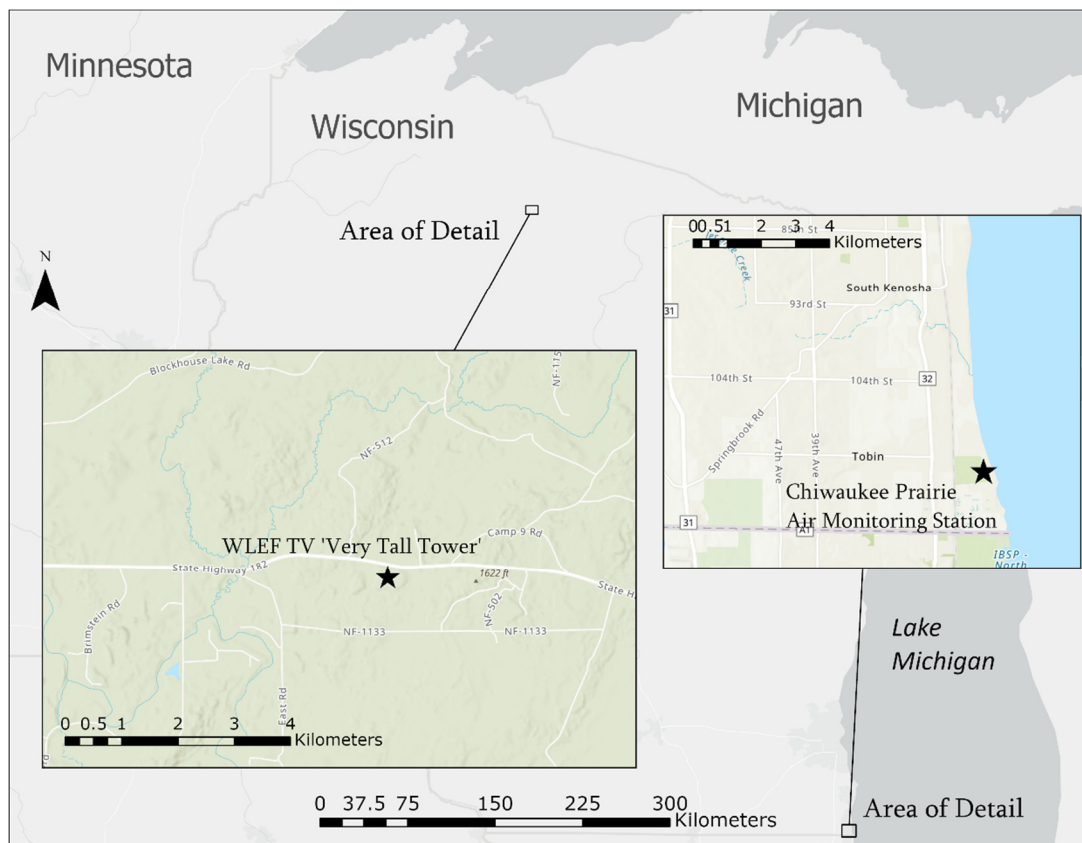
101 The goal of this study is to develop a technique for investigating the vertical profiles of ozone at a shoreline location impacted
102 by high ozone episodes. Chiwaukee Prairie, WI hosts a regulatory site at a shoreline state natural area, which is one of the few
103 in Wisconsin which regularly exceed federal ozone standards and is regularly impacted by lake breeze. The large sources of
104 emissions for ozone precursors are mainly concentrated in the Chicago metro area and the presence of Lake Michigan provides
105 an inverted atmosphere at times in which to trap said pollutants. The role of the inversion over Lake Michigan, the advection
106 of pollutants over Lake Michigan and then back on land during the meso-scale meteorological phenomenon of the Lake Breeze
107 is the focus of the WiscoDISCO field campaigns. We first outline how the instrumentation was tested in a non-lake shore
108 environment during CHEESEHEAD19 and then describe improvements to instrumentation performance for the first
109 WiscoDISCO field campaign in 2020. Here, the UAS-based observations of ozone and meteorological variables were
110 compared to tower observations in a forested environment in 2019 and then ground observations at a Lake Michigan shoreline
111 in 2020 demonstrating improved performance and viability of a UAS atmospheric profiler to investigate lower atmospheric
112 variability at a site impacted by lake breeze and poor air quality.

113 **2 Materials and Methods**

114 **2.1 CHEESEHEAD19 and PÉcorINO Measurement Campaigns**

115 The University of Wisconsin-Eau Claire team joined the Chequamegon Heterogenous Ecosystem Energy-Balance Study
116 Enabled by a High-density Extensive Array of Detectors 2019 (CHEESEHEAD19) campaign (Butterworth et al., 2021) in
117 July 2019 in order to compare UAS-based observations with tower observations made during the first 7-day intensive
118 observation period of the field campaign. CHEESEHEAD19 was the multi-institute campaign that sought to give insight into
119 atmosphere-land exchanges in a temperate mixed forest (Butterworth et al., 2021). The CHEESEHEAD19 domain
120 incorporated a swath of land in the Chequamegon National Forest near Park Falls, WI, where multiple tower, UAS, aircraft,
121 ground, and remote sensing observations were conducted, focused around the 447 m instrumented tower operated by WLEF-
122 TV (45.946 N, 90.273 W) and owned by the State of Wisconsin. Local vehicular traffic at the tall tower site was light and
123 mixed trucking, forestry, and automobile traffic on WI Highway 182 (Figure 1). The tower has been in operation since 1995
124 as a National Oceanic and Atmospheric Administration (NOAA) greenhouse gas tall tower site (LEF) and since 1996 as an
125 Ameriflux eddy covariance site (US-PFa), with sampling inlets and flux measurements currently at 30, 122 and 396 m above
126 ground level. Ozone concentration observations were at two specific heights on the tower (30 m and 122 m) by two
127 instruments: a chemical ionization time-of-flight mass spectrometer (CI-ToFMS, Tofwerk, and Aerodyne) using oxygen anion
128 (O_2^-) ionization chemistry (1 s L.O.D. ~10 ppt) (Novak et al., 2020) and an EPA standard photometric analyzer (L.O.D. 0.5

129 ppb ThermoScientific 49i) (Vermeuel et al., 2021). The fast observations of ozone by the CI-ToFMS instrument were used
130 for flux measurements (Vermeuel et al., 2021). For the purposes of proving the viability of a UAS-mounted ozone
131 measurement, the tower ozone measurements were compared to ozone gradient measurements from the UAS-mounted POM.



132
133 **Figure 1: During the CHEESEHEAD19 and PEcorINO campaigns, measurements were taken at the WLEF TV ‘Very Tall Tower’**
134 **(northern Wisconsin). During the WISCODisco20 campaign, measurements were taken by the Chiwaukee Prairie Air Monitoring**
135 **Station (southeastern Wisconsin). Map was made with ArcPro 2.8 using ESRI basemap data.**

136 A follow-up study Probing Ecosystem Responses Involving Notable Organics (PEcorINO) (Vermeuel et al., 2023) was
137 conducted in September 2020 at the WLEF tower with observations of VOC and ozone at the 30 m inlet (Figure 1). A high-
138 resolution proton-transfer reaction time-of-flight mass spectrometer (HR-PTR-ToFMS) (Vocus; Aerodyne Research Inc. and
139 Tofwerk AG (Krechmer et al., 2018)), collected continuous 10-Hz measurements of VOCs and a photometric analyzer
140 (ThermoScientific 49i) collected 1 Hz O₃ measurements at 30 m. Routine US-PFa site measurements of 10 Hz temperature
141 and 1-Hz measurements of relative humidity (HMP-45C) were also collected during this period.

142 For CHEESEHEAD19, the Yuneec Typhoon H hexa-copter UAS was flown four days in July 2019 (July 8, 11, 12, and 16)
143 during the campaign at the WLEF tower and September 13 and 14, 2020 during PEcorINO. The Typhoon H, owned by UW-
144 Eau Claire, was chosen for this campaign because it was an inexpensive commercial UAS with capability of holding the
145 payload of the POM. Flights in 2019 were conducted in the time window of 11 am - 3 pm local time (CDT) and at 11 am and

146 6 pm CDT in 2020. The Typhoon H was equipped with the POM for each of the flights at the tall tower, and an Internet
147 Systems meteorological sensor, the iMet-XQ2, for the flights on July 16, 2019, and September flights from 2020 (See Figure
148 2a). The iMet-XQ2 sensor was placed on the landing gear of the Typhoon H to balance the payload. The days were chosen for
149 suitable flying conditions without strong winds (< 15 mph gusts) or rainstorms or other precipitation. The Typhoon H was
150 flown from a location roughly 100 ft from the tall tower in different patterns to hover for 5 min at 30 m, 60 m, 90 m and 122
151 m above ground level. Tower gradient uncertainties were determined from 1 standard deviation of the data from 30 and 122
152 m. The instruments sampling at the 122 m and 30 m heights from the tall tower were switched periodically (Vermeuel et al.,
153 2021). The POM ozone data were collected at 10 s intervals and averaged to 5 minutes.

154 Before the CHEESEHEAD19 campaign, numerous test flights were necessary to work out payload distribution and to devise
155 flight strategies. The Typhoon H had an approximate 15-minute flight time per battery with the payload. Each flight of the
156 Typhoon H flights consisted of 2 hovers at different heights for 5 minutes. UAS flight log data were saved and was used as
157 primary source for GPS data. All UAS flights were conducted under Federal Aviation Administration (FAA) Part 107 UAS
158 regulations with a licensed UAS pilot.

159 **2.2 The WiscoDISCO20 Campaign**

160 The purpose of the Wisconsin's Dynamic Influence of Shoreline Circulations on Ozone (WiscoDISCO) campaign was to
161 investigate the marine inversion influence on ozone measurements at the Lake Michigan shoreline by using an UAS at
162 Chiwaukee Prairie Natural Area in Kenosha County, WI. A regulatory monitor at Chiwaukee Prairie managed by the
163 Wisconsin Department of Natural Resources (WiDNR) records some of the highest ozone in the state of Wisconsin and many
164 Wisconsin shoreline Lake Michigan counties are in nonattainment of federal ozone standards (Stanier et al., 2021). Chiwaukee
165 Prairie is located at the border between Wisconsin and Illinois and is situated between the coastal communities of Winthrop
166 Harbor, Illinois, and Pleasant Prairie, Wisconsin. Suburban housing developments and mixed farmland surround the prairie
167 (Figure 1). Local automobile traffic near to the monitor and UAS launch site was light and limited to neighborhood traffic and
168 occasional train traffic.

169 The main goal of this campaign was to capture ozone exceedance days at this site where there was an influence of
170 the lake breeze circulation. Ozone exceedance days are typically those in which the synoptic winds bring air from the south
171 northward with high pressure systems over the Ohio Valley (Hanna and Chang, 1995), which are influenced heavily by
172 Chicago pollution plumes. In this environment, temperature inversions commonly form when near-surface air is chilled by
173 thermal exchange with the comparatively cold water of Lake Michigan and are exacerbated when lake breezes advect this
174 dense but shallow layer of cold air inland (Wagner et al., 2022). The result is a shallow pool of colder, denser air overlain by
175 warmer air aloft, with the inversion defined by the temperature increase with height at the boundary between the dissimilar air
176 masses. Inversions act as a cap on the vertical mixing of air that would otherwise dilute and disperse NO_x and VOCs within
177 these pollution plumes. Thus, these ozone precursors can accumulate in the near-surface air to relatively high concentrations.

178 During WiscoDISCO20 UAS were deployed on June 8, 9 and 15-19, 2020. The WiscoDISCO20 campaign was in
179 collaboration with the Wisconsin Department of Natural Resources' (DNR)'s enhanced monitoring plan for the Chiwaukee
180 Prairie site and included Pandora (Herman et al., 2009) (a ground-based differential optical absorption spectrometer which
181 uses the sun as a light source to obtain total column trace gas measurements) and Doppler lidar observations at the site, provided
182 by the Space Science and Engineering Center at the University of Wisconsin-Madison. The Doppler lidar instruments were
183 deployed on June 9, 2020 and operated continuously throughout the summer. The Pandora instrument is part of the Pandonia
184 Global Network, (Verhoelst et al., 2021) which provides automated measurements of total column and tropospheric column
185 NO₂.

186 A DJI M600 hexa-copter was utilized in a collaborative research endeavor with Purdue University for the WiscoDISCO20
187 campaign with an FAA compliant Part 107 UAS pilot, Joe Hupy. The DJI M600 had an increased payload capacity with its
188 camera removed and the ability to place a top-mount for the sensor package, thus increasing the stability of the payload and
189 providing a longer flight time than the Typhoon H (See Figure 2b). A 3D printed bracket to support the POM was mounted
190 to the top of the vehicle. The inlet filter cartridge for the POM was held at a position with the least influence from propeller
191 wash at the center of the top position of the UAS with a ~6 cm inlet tube. The iMet-XQ2 sensor was mounted to the bracket
192 and secured with cable ties (See SI: Figure S2). During WiscoDISCO20, a series of flights were conducted to produce an
193 atmospheric vertical profile with fixed altitudes where the UAS hovered for 5 minutes at each designated altitude. The flight
194 times were approximately 15-20 minutes where the UAS would ascend for 15 m altitude increments where it would hover
195 for 5 minutes. In an approximate 1.25-hour time window, 8 heights were sampled from 0-122 m AGL with 3 individual
196 flights (See SI: Table S1). Flights were conducted from a gravel road inside of the Chiwaukee Prairie State Natural Area,
197 with two focused vertical profile sampling periods: one in the morning at approximately 7-9 am local time (CDT) and one in
198 the afternoon at approximately 2-4 pm local time (CDT).



199

Figure 2. a) Typhoon H UAS with mounted POM and iMet-XQ2 as flown during CHEESEHEAD-19 in 2019. POM was housed in foam for vibration dampening. b) Top mounted iMet-XQ2 and POM on a DJI M600 as flown in Sept. 2020 for WiscoDISCO20. The inlet to the POM is held up with a bracket to hold the inlet filter assembly (blue and white).

200

201 **2.3 Personal Ozone Monitor, POM**

202 The 2B Tech personal ozone monitor, POM, measured ozone concentrations via UV absorption spectroscopy, which is
203 designed to account for a known interference with humidity in the atmosphere (Wilson and Birks, 2006). The POM measures
204 ozone concentrations by calculating the difference in absorption between a whole air and a scrubbed ozone air sample in-series
205 with one optical cell. The POM operates with an in-series duty cycle of measuring the whole air sample for 5 seconds and an
206 ozone-scrubbed background air sample for another 5 seconds in the same optical cell (Andersen et al., 2010). This differs from
207 current robust ground analysers, such as the ThermoScientific 49i, which use dual optical cells, one chamber of whole air and
208 another chamber with ozone scrubbed out to measure a real-time background interference in the absorption signal (Ollison et
209 al., 2013) (Wilson and Birks, 2006). This duty cycle must be considered when the POM is on a moving platform, as the air
210 sampled in the first 5 seconds must be representative of the air sampled in the second 5 seconds for each measurement, therefore
211 slow movement of the UAS during sampling was preferred. For all measurements described here, the UAS was held at one
212 altitude for 5 minutes to collect representative data from that airmass. The absorption spectroscopy principle behind the POM

213 with the active background humidity subtraction has a higher specificity to ozone than other light-weight electrochemical
214 sensors(Kim et al., 2018). The POM was calibrated with the 2B Tech Model 309 transfer standard ozone generator within 24
215 hours of UAS flights during CHEESEHEAD19. The POM was placed in a foam case to dampen any vibrations associated
216 with the UAS to which it was fastened. The filter on the POM was used for all flights to protect the optical cell from
217 atmospheric particles and debris. The POM was independently powered by lithium-ion batteries. During WiscoDISCO20, the
218 POM was calibrated with the Model 309 ozone generator within 2 hours of each atmospheric profile series of UAS flights.
219 Zero drift of the POM was monitored by collecting scrubbed-ozone data using a cartridge ozone scrubber in between flights.
220 The 2B Tech listed POM accuracy and precision are given as 1.5 ppb or 2% of observations whichever is highest. For the
221 range of observations in this study, the accuracy and precision ranged from 1.5 ppb for many morning observations to up to
222 2.1 ppb for high ozone afternoon observations.

223 **2.4 iMet-XQ2**

224 The iMet-XQ2 sensor is lightweight and portable which allows it to measure temperature (bead thermistor), relative
225 humidity (capacitive), and pressure (piezoresistive) along with recording GPS data with its own internal storage and power
226 systems. The International Met Systems listed iMet-XQ2 accuracy and resolution of ± 0.3 °C and 0.01 °C for temperature, $\pm 5\%$
227 and 0.1% for relative humidity, ± 1.5 hPa and 0.01 hPa for pressure, and an accuracy of 12 m for vertical GPS data. The data
228 were extracted from the iMet-XQS after each flight.

229 Previous studies have evaluated the accuracy of the iMet-XQ2 on UAS platforms (Kimball et al., 2020; Inoue and
230 Sato, 2022). Kimball et al. executed an exhaustive study on the performance of the iMet-XQ on a UAS in certain solar radiation
231 and wind speed conditions. While they found that under low solar radiation, the accuracy and precision of the temperature
232 measurement followed the listed accuracy and precision, with some direct solar radiation, higher wind speeds on the thermistor
233 allowed for improved precision of the measurements. In cold conditions, shielding the thermistor from both solar radiation and
234 heating from the UAS is important (Inoue and Sato, 2022). Sensor position on the UAS has been found to be important for
235 preventing additional bias from motor heating and propellor wash if the sensor is placed too close to UAS motors (Greene et
236 al., 2019). For this study, a lower accuracy of the iMet-XQ was considered reasonable to ascertain the vertical profile structure
237 of the atmosphere at a shoreline location, if the solar radiation conditions and flight conditions were similar throughout the
238 data collection flight.

239 **3 Results and Discussion**

240 **3.1 UAS to Tower Comparisons**

241 During the CHEESEHEAD19 campaign, an intercomparison was conducted between the observations of ozone from the
242 WLEF tall tower and UAS.. The tall tower ozone measurements were from either a ThermoFischer 49i photometric analyzer
243 or a CI-ToFMS instrument. Each sampled air from either the 122 m or 30 m inlet simultaneously, and source inlets (i.e. sampled

244 heights) were switched between instruments periodically. The absolute ozone concentrations at the 122 m and 30 m heights
 245 from the tall tower ranged from mid-day highs of 40-60 ppb. Tower ozone gradients were calculated as the difference between
 246 the ozone measured at 122 m and 30 m inlet heights. These tower observations were compared to the gradient ozone
 247 observations made by hovering the UAS at the 122 m and 30 m altitudes for 5 minutes each. The gradient ozone observations
 248 reproduced the reported ozone gradients on the tall tower within the considerable uncertainty (See Table 1). The absolute
 249 concentrations from the POM were as much as 20 ppb higher than the tower observations (See SI: Figure S3), with tower
 250 observations from both the 49i and TOF considered to be the more reliable measurements with consistent calibration
 251 procedures and low detection limits (Vermeuel et al., 2021; Vermeuel et al., 2023). Technically the overall comparison between
 252 tower gradients and UAS gradients show agreement; however, the considerable uncertainties make POM gradients from 8 and
 253 11 July indistinguishable from zero (See Table 1). This evaluation demonstrated a likely source of inaccuracy with POM ozone
 254 observations, with significant offset from the absolute tower observations. These inaccuracies have since been attributed to
 255 zero-point drift of the POM, which was substantiated by further laboratory experiments on calibration conditions of the POM.
 256 Those experiments showed differences in calibrations due to different sources of power to the POM (batteries versus wall-
 257 power). Large noise in the POM observations was attributed to disrupted airflow from propeller wash which was exacerbated
 258 by the bottom-mount of the POM on the UAS, as observed as higher noise during take-off and at the start of every hover.

259 Improvements to the UAS sensor package for the WiscoDISCO20 system were developed as a result of these findings
 260 as follows: a) the POM was mounted at the top of a larger UAS with the inlet positioned to the center of a larger, more robust
 261 platform, b) the POM was calibrated with the same independent POM battery source as the flights and calibrations were
 262 conducted within 2 hours of every flight and c) zero drift was monitored by placing an in-line ozone scrubber on the POM
 263 inlet directly after each flight for 5 minutes. The temperature and relative humidity measurements observed from the UAS
 264 using the iMet were found to vary from the tower measurements by no more than 1.7°C for temperature and 8% RH (See Table
 265 2).

267 **Table 1: Comparison of ozone gradients made from Tall Tower at Park Falls and UAS-based POM during CHEESEHEAD-19.**
 268 **Ozone gradient, ΔO_3 , calculated as measured O_3 at 122 m – O_3 at 30 m. The tower measurements were selected as coincident with**
 269 **UAS-mounted POM measurements. Uncertainties reported are propagated from 1 standard deviation at each altitude.**

Day-Month- Year of Flight	POM UAS	Tower
	$\Delta O_3 \pm \sigma$ (ppb)	$\Delta O_3 \pm \sigma$ (ppb)
08-Jul-19	-5.9 ± 9.6	1.0 ± 1.1
11-Jul-19	11.9 ± 21.7	8.7 ± 0.8
12-Jul-19	16.1 ± 13.2	9.1 ± 1.3

270
271
272
273
274
275
276
277

Table 2: Comparison of average air temperature and relative humidity made from Tall Tower at Park Falls and iMet-XQ during CHEESEHEAD-19 and PECOINO in 2020. The average Tower temperatures at the 30-meter inlet were computed at the time intervals when the UAS altitude was 30 meters AGL. The iMET and Tower data were evaluated at 1 Hz, therefore approximately n=300 for each 5-min hover period.

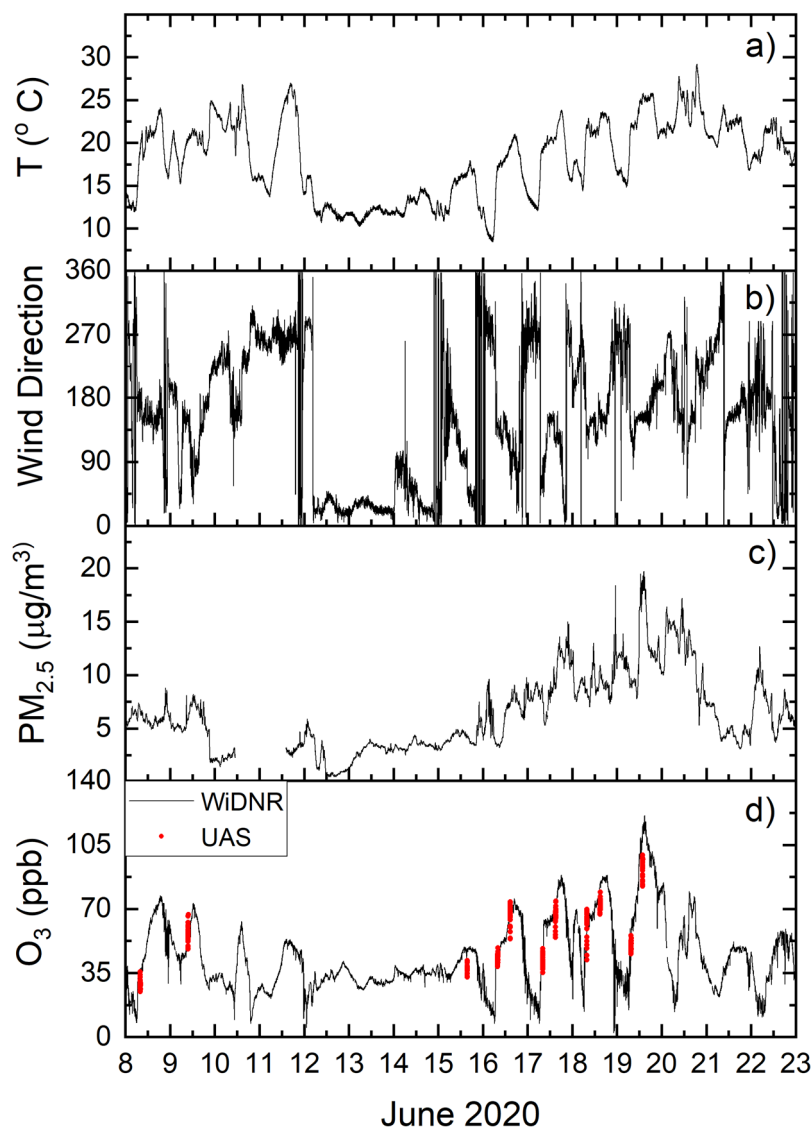
Day-Month- Year of Flight	Altitude A (meters)	iMet UAS T ± σ (°C)	Tower T ± σ (°C)	iMet UAS RH ± σ (%)	Tower RH ± σ (%)
16-Jul-19	30	25.0 ± 0.4	24.43 ± 0.07	61.2 ± 1.3	66.8 ± 0.4
13-Sep-20	30	15.5 ± 0.3	13.8 ± 0.9	68.9 ± 0.8	76.7 ± 5.5
14-Sep-20	30	13.5 ± 0.8	13.0 ± 0.8	63.0 ± 6.4	61.5 ± 6.8

278

279 3.2 Observations at Lake Michigan Shoreline: WiscoDISCO20 UAS to Ground Comparisons

280 The viability for UAS-mounted ozone observations to capture low-altitude features in ozone is well-matched to the small-
281 scale vertical structure of marine layer ozone concentrations in a near-shore environment. For the June 2020 observations, the
282 UAS platform was the DJI M600 with a top-mounted bracket for positioning the filter cartridge for the POM in a space for
283 minimal disruption of the air mass from propeller wash. The iMet-XQ2 sensor was mounted to this bracket to the side of the
284 POM (See SI: Figure S2). The DJI M600 was flown at the Chiwaukee Prairie State Natural Area to capture shoreline airmasses
285 impacted by lake breeze onshore flow during time of high ozone. The week of June 15-19, 2020, provided ideal conditions for
286 high ozone and lake breeze conditions (as seen in Figure 3) where daytime winds shifted regularly to southeasterly and daily
287 maximum temperatures increased throughout the week (See SI for identification of lake breeze from GOES-East satellite
288 imagery). Most days during the week of June 15-19 had observable cumulus cloud suppression fronts over land near to the
289 shoreline of Lake Michigan which is indicative of marine air incursion over land (see SI: Figures S4-S5). Particulate matter
290 concentrations also increased during the week. The UAS was flown in a 2-hour window to capture morning and afternoon

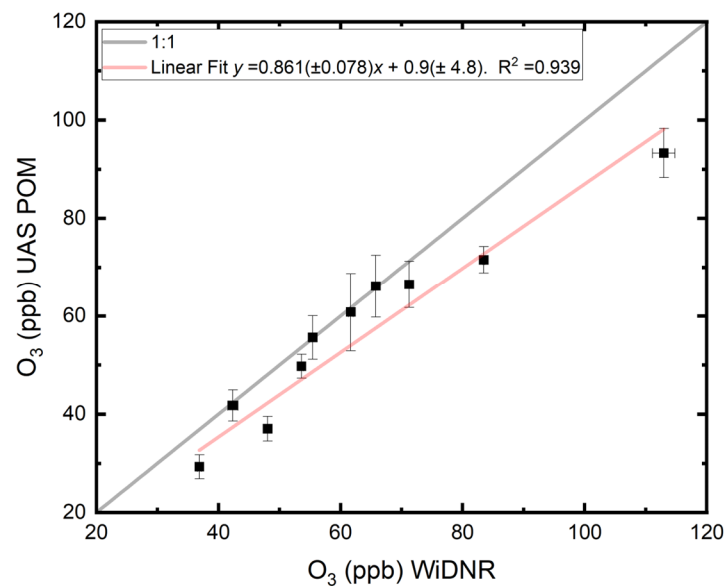
291 vertical atmospheric profiles. A single battery flight of the UAS accounted for 3-4 hover heights and multiple sets of batteries
292 were used to hover for 10 total points to get a vertical distribution.



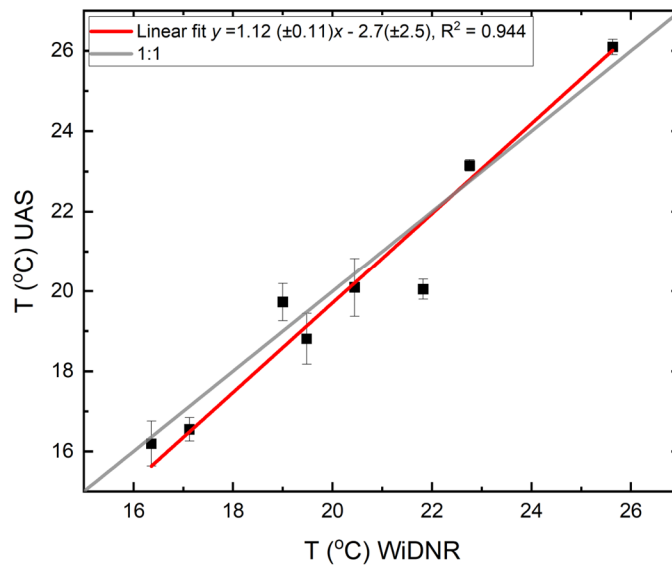
293
294 **Figure 3: June 8-22, 2020 a) temperature in °C b) wind direction, c) $PM_{2.5}$ in $\mu g/m^3$ and d) O_3 as measured at the WDNR ground**
295 **station (black) and on the UAS via POM (red).**

296 The accuracy of the ozone concentration, temperature, and relative humidity (RH) observations made aloft on the UAS was
297 evaluated by comparing the lowest altitude hover altitude at 9 meters above ground level (m AGL) to 1-minute data from the
298 local air monitoring station in Chiwaukee Prairie (AIRSID# 55-059-0019). The uncertainty in the UAS-mounted POM was

299 determined to be the 1 standard deviation in the averaged 10 s data. A regression analysis of the two observations is given in
300 Figure 4a; these data are strongly correlated as the R^2 value is 0.939. The linear fit to the graph is weighted by the highest
301 ozone data and the RMSD = 5.3 ppb. Some disagreement could be from the discrepancy in altitudes for the two observations
302 (the DNR inlet is at 4.5 m in comparison to the first altitude for hovers at 9 m), or to accuracy issues with the zero drift as
303 observed during CHEESEHEAD-19. A similar comparison was conducted for the iMet temperature measured at the lowest
304 hovering altitude (approx. 9 m) with ground temperatures (Figure 4b) with an agreement at $R^2= 0.944$. With these added
305 observations, the accuracy for the O_3 concentrations via UAS-mounted POM are considered accurate within 10 ppb, and the
306 iMet temperatures within 11 %. This figure has some similarities for the Li et al. (Li et al., 2020) figure 5a, where they saw a
307 linear fit of $0.7x - 7$ for a POM correlation to a regulatory ozone measurement instrument standard. The difference between
308 our measurement and theirs is that we see more observations along the 1:1 line with higher ozone concentrations deviating the
309 most from the center line, whereas Li et al. (2020) showed a consistent linear response at $\sim 70\%$ of the regulatory O_3
310 measurement.



311 a)



312 b)

313

314 **Figure 4: a) Intercomparison O₃ UAS POM measurements in comparison to O₃ WiDNR Chiwaukee Prairie measurements on June**
 315 **8, 9, 15-19 2020. The 5- minute average WiDNR and UAS POM data from the lowest hovering altitude is with uncertainties as 1σ**
 316 **from the mean. The grey line demonstrates a 1:1 line and the red line depicts a linear regression fit (R² = 0.939), with a fit of [O₃ POM**
 317 **]= 0.861 (±0.078) [O₃ WiDNR] + 0.9 (± 4.8). b) Intercomparison of temperature from lowest altitude reading from the UAS-mounted**
 318 **iMet-XQ2 and the WiDNR ground station. Red line indicates the linear regression (T_{iMET-XQ2} = 1.12 (±0.11) T_{WiDNR} - 2.7(±2.5), R² =**
 319 **0.944) and the gray line is 1:1 fit.**

320

321 3.3 Case study: Low Altitude Gradients at the Lake Michigan Shoreline

322 The week of June 15-19, 2020 had 4 days where O₃ concentrations exceeded 70 ppb (Figure 3 d). The dominant winds were
 323 from the south and lake breezes were observed on all days that week (Figure 3 b), which are conditions conducive to higher
 324 ozone concentrations along the Lake Michigan shoreline due to Chicago emissions getting trapped over Lake Michigan during
 325 optimal conditions for photochemical production of ozone and then advecting ozone back on land at the shoreline (Vermeuel
 326 et al., 2019; Abdi-Oskouei et al., 2020; Cleary et al., 2022b; Baker et al., 2023). The conditions near Lake Michigan were
 327 consistently sunny at the shoreline with some evidence for cumulus cloud formation inland on June 19, 2020 often used as a
 328 identifying signature of lake breeze from satellite observations (Levy et al., 2010; Sills et al., 2011).

329 Vertical profiles for UAS flights were constructed using hovering altitudes of the UAS and time stamps for each altitude to
 330 determine observed average O₃, temperature, pressure and relative humidity (RH) for each altitude. Because of limited battery
 331 time, each vertical profile was constructed from 3-4 hovering altitudes during 3 separate 20-minute flights, covering a time
 332 window of approximately 1.25 hours (See SI Table S2). Figure 5 depicts vertical profiles of potential temperature overlaid

333 with ozone concentrations through the week of June 15-19, 2020. Every day shows an inverted stable atmosphere. Some days
334 show a well-mixed buoyant internal boundary layer in the lowest 40-100 m AGL (Figure 5) where the potential temperature
335 is close to a vertical line with respect to altitude, particularly in the June 18 and 19 afternoon flights. This discontinuity of most
336 vertical profiles exists where the lowest 40-60 m AGL is closer to a more vertical potential temperature profile, which we refer
337 to as the internal boundary layer, followed by a steep inversion aloft, most pronounced in June 16, 17, and 18 afternoons with
338 a gradient of 5 K or more within 60-100 m AGL. The morning of June 18 (Fig 5-c) was the only day to show a steep inversion
339 down to the surface with no discontinuity. Ozone concentrations in all ascents had maximum observations below the maximum
340 altitude of the flight. Ozone concentrations tended to be highest near areas of steep inversion (June 15, June 17 am and pm,
341 and June 18 pm flights) or near/within the internal boundary layer (June 16 pm, June 19) except on June 18 in the morning
342 when ozone concentrations were highest at the lowest altitudes when the inversion extended to the surface. For all 5 days,
343 observed afternoon maximum ozone concentrations were observed at higher altitudes than adjacent to the surface (Figures 5
344 a-e). The higher ozone concentrations in the vertical profiles tended to be at or near the maximum inversion generally in the
345 region of 40-60 m AGL.

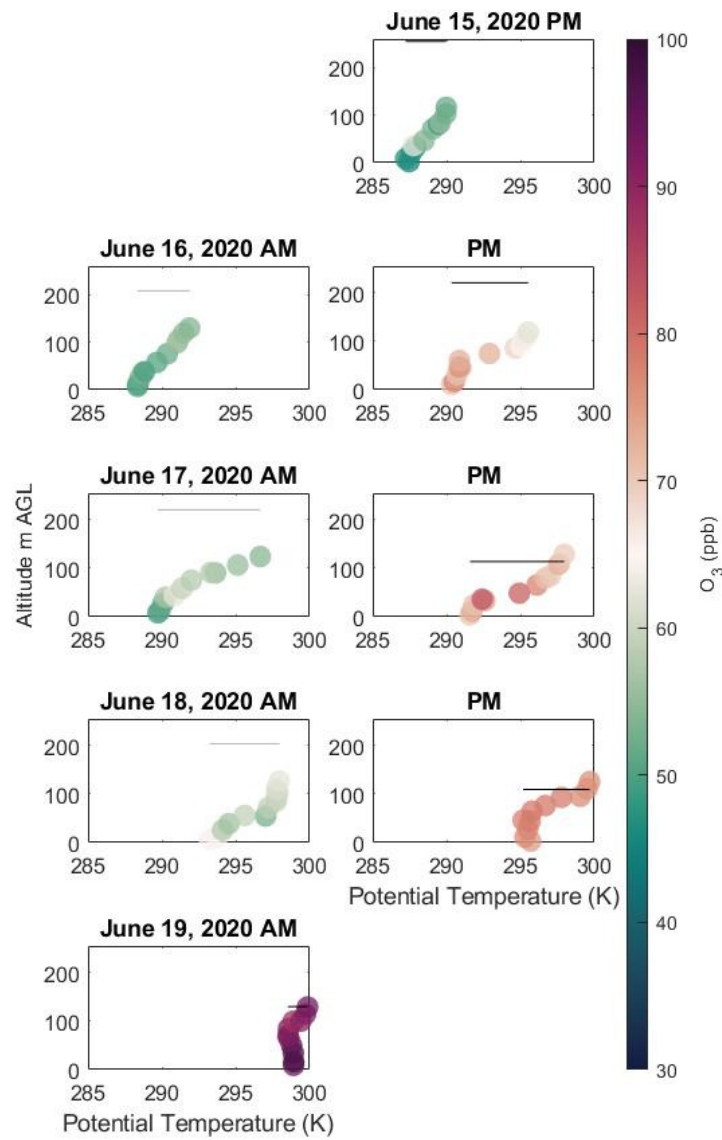
346 The variation in height of the steep inversion layer is evident in the day-to-day differences, from as low as 40 m AGL (June
347 15, 16, and 17) to as high as 100 m AGL on June 19. Morning to afternoon differences on July 16 and 17 show a steeper
348 gradient in temperature later in the afternoon with not much change in the inversion height. By contrast, on the morning of
349 July 18, the vertical profile of temperature shows an inversion starting at the surface (Figure 5d) and by the afternoon the
350 inversion height starts at 60 m AGL. In comparison, turbulent kinetic energy (TKE) based boundary layer depths given by the
351 High-Resolution Rapid Refresh (HRRR) (Dowell et al., 2022) atmospheric model outputs extend from 80 to 250 m AGL for
352 this location, not as low as the data in Figure 5. HRRR boundary layer height is a metric which addresses how photochemical
353 models are treating vertical profiles when computing photochemical ozone production. The use of the HRRR boundary layer
354 height highlights the sub-grid scale of the vertical profiling, which indicates that UAS observations can sample important
355 properties of the marine air incursion of a lake breeze. The lower boundary layer heights in the afternoon in comparison to the
356 morning are proposed to arise from stronger synoptic winds degrading the inversion from above (Lyman and Tran, 2015).
357 Doppler lidar measurements (which cannot make observations below 100 m AGL) show high aerosol loading in the afternoons
358 at altitudes close to the ~100 m cut-off altitudes below which the instrument has a dead zone, which may correspond to
359 continued inversion up to 200 m or more. The UAS observations give a complementary measurement to indicate the region of
360 inversion and the compositional layering below, within, and above the inversion to demonstrate a more complicated picture of
361 mixing and vertical stratification in the lower atmosphere. While these measurements may not adequately address exactly why
362 models do not represent the shoreline effectively (See SI Figure S6), they can shed light on the required resolution and vertical
363 structure that encompasses plume volume within an inverted atmosphere near Lake Michigan.

364 The UAS observations at Chiwaukee Prairie shown here demonstrate a very shallow internal boundary layer (40-100
365 m AGL) developed over land underneath the temperature inversion (modeled boundary layer heights 80-250 m AGL), where
366 ozone is found to be in highest abundance near the maximum inversion. On two days with the highest internal boundary layer

367 height, ozone concentrations were highest within the internal boundary layer, suggesting that an extended internal boundary
368 layer height over land could possibly play a role in transport of pollutants in the marine layer. However, more observations of
369 atmospheric profiles of ozone and meteorology are required over land and over water to better characterize this transitional
370 environment.

371 The work by Li et al. (2020) described use of POM and particle observation on a fixed-wing UAS flying at a speed
372 of 150 km/hr and compared measurements from those instruments to regulatory instruments on a tethered airship and
373 addressed intercomparison with the POM and a regulatory ozone measurement instrument (O₃42M from ESA). They used an
374 insulated box for the POM and were able to show high correlation with a regulatory monitor, but with an offset. Their
375 conclusions are that the POM measures atmospheric variability consistent with a regulatory monitor but demonstrates a
376 negative bias. Here, we flew the POM at a much lower flight speed, and only averaged data from a single hovered point at
377 which we stayed for 5 minutes each flight. This was to address the duty-cycle limitations of the POM with the on-off in
378 series subtraction of the water vapor absorption. Li et al. address only that the regulatory monitor they used for comparison
379 which employed an in-line heating method for removing water vapor interference, instead of a dual-cell active subtraction in
380 parallel as is typical for other regulatory monitors. While Li et al. 2020 demonstrated some correlation between RH and
381 variability between the UAS-mounted POM and tethered-airship-platform regulatory monitors, they do show that vertical
382 gradients can be captured by UAS and tethered airship, but with discrepancies in location of planetary boundary layer. This
383 is consistent with our observations that the gradient observations from UAS are in agreement (with high variability) with
384 tower-based observations in the lowest 120 m AGL. What we cannot account for here is the difference in POM variability on
385 a UAS which hovers for 5 minutes in comparison to a fixed-wing travelling at 150 km hr⁻¹, which may also lead to additional
386 variability in the measurement due to inlet pressure changes and optical cell vibrations. Additional improvements to the
387 POM performance could arise from a) thermal insulation and b) a slow constant ascent instead of hovering and are intended
388 for future studies. Additional improvements to the iMET-XQ2 performance could arise from a slow ascent (to assist in
389 aspirating the thermistor) and shielding the iMET to account for solar irradiation of the sensors.

390 The feasibility of using UAS in shoreline environments depends on the vertical scale of the phenomenon, the UAS
391 flight time and requisite battery life for such UAS observations and the legal flight conditions within each municipality. Some
392 researchers have successfully used UAS for vertical ozone profiles up to 1000 m (Chen et al., 2022; Wu et al., 2021), tethered
393 balloons (Li et al., 2020; Chen et al., 2022) and thermally insulated a UAS-mounted POM in the winter (Chen et al., 2020;
394 Chen et al., 2019). The scales of sea breeze influence on vertical profiles have ranged from 400-600 m AGL at coastal locations
395 in Nova Scotia (Gong et al., 2000), 600-800 m AGL at coastal locations in China (Wu et al., 2010) and 400-800 m AGL in
396 lake breeze influenced locations in Saskatchewan (Sun et al., 1998). The lake breeze vertical dimensionality near Lake
397 Michigan has been shown to have large effects at altitudes from 50-500 m AGL from crewed aircraft (Stanier et al., 2021;
398 Cleary et al., 2022b), remote sensing (Wagner et al., 2022) and UAS studies (Tirado et al., 2023).
399



400

401 **Figure 5: Altitude (m AGL) versus potential temperature (K) with O₃ (ppb) for a) June 15 flights, June 16 b) morning, and c)**
 402 **afternoon flights, June 17 d) morning and e) afternoon flights, June 18 f) morning and g) afternoon flights, and h) June 19 afternoon**
 403 **flights. All times in CDT (2020). Grey and black bars indicate HRRR boundary layer heights for morning and afternoon,**
 404 **respectively.**

405

406 **4 Conclusions**

407 An UAS atmospheric profiler was tested in comparison to tower-based instrumental observations indicating a need for
408 careful adjustments to operating parameters for the ozone measurements. Improvements including a top-mount for the sensor
409 package, a larger UAS and higher frequency calibrations and zero-drift checks were shown to improve overall accuracy of the
410 ozone observations near a ground air monitoring station. The improved vertical atmospheric profiler was shown to capture
411 atmospheric variability in the lowest 120 m of the atmosphere at a Lake Michigan shoreline region, demonstrating a feasible
412 use for UAS in atmospheric sampling to connect the scales of ground-based observations and tower or remote sensing aloft.
413 These observations are the first UAS observations of ozone near Lake Michigan that document the over-land penetration of
414 the marine layer and gradients in ozone within it. This work highlights the necessity for higher vertical resolution in
415 observations in this shoreline location to inform improvements to how air quality models represent the stratification and mixing
416 of air parcels at locations like these.

417 Suggestions for further improvements: in this study, the POM performance on UAS was improved by inlet positioning
418 and slow flight parameters, top-mount placement on a robust UAS and increasing the rate of calibrations to pair each calibration
419 with specific battery power source improved the precision and accuracy. However, added thermal insulation, as described by
420 Li et al, appears another promising additional consideration for improved performance of the POM on UAS. The POM appears
421 to be a robust enough instrument for course atmospheric measurements in the atmosphere (to 2 ppb precision or 2% of reading)
422 but integration onto a UAS should be carefully considered. A wider variety of studies have been conducted on iMET
423 performance on UAS (Kimball et al., 2020; Inoue and Sato, 2022; Greene et al., 2019).

424 **Appendices**

425 Supplemental Info

426

427 **Data Availability**

428 A data repository was generated for CHEESEHEAD19 at: https://data.eol.ucar.edu/master_lists/generated/cheesehead/ (last
429 accessed 7/6/2023).

430 A data repository was generated for the WiscoDISCO 2020 field campaign at:
431 <https://zenodo.org/communities/wiscodisco2020/> (last accessed 7/6/2023). Dataset available at DOI:
432 10.5281/zenodo.8118176. Each data file is in a .txt tab delimited structure with descriptive column titles. Any data file with a
433 full suite of data from both iMET and POM instruments is given without a qualifier. On days when data was collected from
434 one of the instruments, the file names indicate them as such.

435 **Author Contributions**

436 JR, BK, MPV and KK contributed to data acquisition, data analysis and manuscript writing. WM, SZ, and AV contributed to
437 data analysis. GP and TW contributed to data acquisition and manuscript writing and editing. AD, TB, and RBP contributed
438 to field campaign planning and manuscript editing and writing. JPH contributed to field campaign planning, data analysis and
439 manuscript writing and editing. PAC contributed to field campaign management, data acquisition, data analysis, manuscript
440 writing and editing.

441 **Competing Interests**

442 The contact author has declared that none of the authors has any competing interests.

443 **Acknowledgements**

444 University of Wisconsin -Eau Claire team acknowledges funding from the Office of Research and Sponsored Programs
445 Faculty/Student Research Collaboration Grants through Blugold differential tuition. This research is funded through the
446 National Science Foundation Grant AGS-1918850. Ankur Desai coordinated the efforts for CHEESEHEAD19 and
447 acknowledges funding from NSF AGS-1822420 and the Dept of Energy Ameriflux Network Management Program award to
448 the ChEAS core site cluster. Any opinions, findings, and conclusions or recommendations expressed in this material are those
449 of the author(s) and do not necessarily reflect the views of the National Science Foundation. Ancestral & Indigenous Lands
450 Acknowledgement: We acknowledge that our research took place at the ancestral lands of the Ojéhéthi Šakówiŋ,
451 Anishinabewaki, Ho-Chunk, Myaamia, Potawatomi, Kaskaskia, Peoria and Kiikaapoi people.

452 **References**

453

454

455 Abdi-Oskouei, M., Carmichael, G., Christiansen, M., Ferrada, G., Roozitalab, B., Sobhani, N., Wade,
456 K., Czarnetzki, A., Pierce, R. B., Wagner, T., and Stanier, C.: Sensitivity of Meteorological Skill to
457 Selection of WRF-Chem Physical Parameterizations and Impact on Ozone Prediction During the Lake
458 Michigan Ozone Study (LMOS), *Journal of Geophysical Research-Atmospheres*, 125,
459 10.1029/2019jd031971, 2020.
460 Adkins, K. A. and Sescu, A.: Observations of relative humidity in the near-wake of a wind turbine using
461 an instrumented unmanned aerial system, *Int. J. Green Energy*, 14, 845-860,
462 10.1080/15435075.2017.1334661, 2017.
463 Andersen, P. C., Williford, C. J., and Birks, J. W.: Miniature Personal Ozone Monitor Based on UV
464 Absorbance, *Analytical Chemistry*, 82, 7924-7928, 10.1021/ac1013578, 2010.

465 Baker, K. R., Liljegren, J., Valin, L., Judd, L. M., Szykman, J., Millet, D. B., Czarnetzki, A., Whitehill,
466 A. R., Murphy, B. P., and Stanier, C.: Photochemical model representation of ozone and precursors
467 during the 2017 Lake Michigan Ozone Study (LMOS), *Atmospheric Environment*, 293, 119465,
468 <https://doi.org/10.1016/j.atmosenv.2022.119465>, 2023.

469 Banta, R. M., Senff, C. J., Nielsen-Gammon, J., Darby, L. S., Ryerson, T. B., Alvarez, R. J., Sandberg,
470 S. R., Williams, E. J., and Trainer, M.: A bad air day in Houston, *Bulletin of the American*
471 *Meteorological Society*, 86, 657-+, 10.1175/bams-86-5-657, 2005.

472 Beekmann, M., Ancellet, G., Martin, D., Abonne, C., Duverneuil, G., Eidelman, F., Bessemoulin, P.,
473 Fritz, N., and Gizard, E.: INTERCOMPARISON OF TROPOSPHERIC OZONE PROFILES
474 OBTAINED BY ELECTROCHEMICAL SONDES, A GROUND-BASED LIDAR AND AN
475 AIRBORNE UV-PHOTOMETER, *Atmospheric Environment*, 29, 1027-1042, 10.1016/1352-
476 2310(94)00336-j, 1995.

477 Bell, M. L., Peng, R. D., and Dominici, F.: The exposure-response curve for ozone and risk of mortality
478 and the adequacy of current ozone regulations, *Environmental Health Perspectives*, 114, 532-536,
479 10.1289/ehp.8816, 2006.

480 Blaylock, B. K., Horel, J. D., and Crosman, E. T.: Impact of Lake Breezes on Summer Ozone
481 Concentrations in the Salt Lake Valley, *Journal of Applied Meteorology and Climatology*, 56, 353-370,
482 10.1175/jamc-d-16-0216.1, 2017.

483 Brauner, E. V., Karotki, D. G., Frederiksen, M., Kolarik, B., Spilak, M., Andersen, Z. J., Vibenholt, A.,
484 Ellermann, T., Gunnarsen, L., and Loft, S.: Residential ozone and lung function in the elderly, *Indoor*
485 *and Built Environment*, 25, 93-105, 10.1177/1420326x14539339, 2016.

486 Butterworth, B. J., Desai, A. R., Metzger, S., Townsend, P. A., Schwartz, M. D., Petty, G. W., Mauder,
487 M., Vogelmann, H., Andresen, C. G., Augustine, T. J., Bertram, T. H., Brown, W. O. J., Buban, M.,
488 Cleary, P., Durden, D. J., Florian, C. R., Iglinski, T. J., Kruger, E. L., Lantz, K., Lee, T. R., Meyers, T.
489 P., Mineau, J. K., Olson, E. R., Oncley, S. P., Paleri, S., Pertzborn, R. A., Pettersen, C., Plummer, D.
490 M., Riihimaki, L., Ruiz Guzman, E., Sedlar, J., Smith, E. N., Speidel, J., Wagner, T. J., Wang, Z.,
491 Wanner, L., White, L. D., Wilczak, J. M., Wright, D. B., and Zheng, T.: Connecting land-atmosphere
492 interactions to surface heterogeneity in CHEESEHEAD19, *Bulletin of the American Meteorological*
493 *Society*, <https://doi.org/10.1175/BAMS-D-19-0346.1>, 2021.

494 Chai, T., Kim, H. C., Lee, P., Tong, D., Pan, L., Tang, Y., Huang, J., McQueen, J., Tsidulko, M., and
495 Stajner, I.: Evaluation of the United States National Air Quality Forecast Capability experimental real-
496 time predictions in 2010 using Air Quality System ozone and NO₂ measurements, *Geoscientific Model*
497 *Development*, 6, 1831-1850, 10.5194/gmd-6-1831-2013, 2013.

498 Chandrasekar, A., Philbrick, C. R., Doddridge, B., Clark, R., and Georgopoulos, P.: A comparison study
499 of RAMS simulations with aircraft, wind profiler, lidar, tethered balloon and RASS data over
500 Philadelphia during a 1999 summer episode, *Atmospheric Environment*, 37, 4973-4984,
501 10.1016/j.atmosenv.2003.08.030, 2003.

502 Chen, L., Pang, X. B., Li, J. J., Xing, B., An, T. C., Yuan, K. B., Dai, S., Wu, Z. T., Wang, S. Q., Wang,
503 Q., Mao, Y. P., and Chen, J. M.: Vertical profiles of O₃, NO₂ and PM in a
504 major fine chemical industry park in the Yangtze River Delta of China detected by a sensor package on
505 an unmanned aerial vehicle, *Science of the Total Environment*, 845, 10.1016/j.scitotenv.2022.157113,
506 2022.

507 Chen, Q., Li, X. B., Song, R. F., Wang, H. W., Li, B., He, H. D., and Peng, Z. R.: Development and
508 utilization of hexacopter unmanned aerial vehicle platform to characterize vertical distribution of
509 boundary layer ozone in wintertime, *Atmos. Pollut. Res.*, 11, 1073-1083, 10.1016/j.apr.2020.04.002,
510 2020.

511 Chen, Q., Wang, D. S., Li, X. B., Li, B., Song, R. F., He, H. D., and Peng, Z. R.: Vertical
512 Characteristics of Winter Ozone Distribution within the Boundary Layer in Shanghai Based on
513 Hexacopter Unmanned Aerial Vehicle Platform, *Sustainability*, 11, 10.3390/su11247026, 2019.

514 Chilson, P. B., Bell, T. M., Brewster, K. A., de Azevedo, G. B. H., Carr, F. H., Carson, K., Doyle, W.,
515 Fiebrich, C. A., Greene, B. R., Grimsley, J. L., Kanneganti, S. T., Martin, J., Moore, A., Palmer, R. D.,
516 Pillar-Little, E. A., Salazar-Cerreno, J. L., Segales, A. R., Weber, M. E., Yearly, M., and Droegemeier,
517 K. K.: Moving towards a Network of Autonomous UAS Atmospheric Profiling Stations for
518 Observations in the Earth's Lower Atmosphere: The 3D Mesonet Concept, *Sensors*, 19,
519 10.3390/s19122720, 2019.

520 Cleary, P. A., de Boer, G., Hupy, J. P., Borenstein, S., Hamilton, J., Kies, B., Lawrence, D., Pierce, R.
521 B., Tirado, J., Voon, A., and Wagner, T. J.: Observations of the Lower Atmosphere From the 2021
522 WiscoDISCO campaign, *Earth System Science Data*, 14, 2129-2145, [https://doi.org/10.5194/essd-14-](https://doi.org/10.5194/essd-14-2129-2022)
523 [2129-2022](https://doi.org/10.5194/essd-14-2129-2022), 2022a.

524 Cleary, P. A., Fuhrman, N., Schulz, L., Schafer, J., Fillingham, J., Bootsma, H., McQueen, J., Tang, Y.,
525 Langel, T., McKeen, S., Williams, E. J., and Brown, S. S.: Ozone distributions over southern Lake
526 Michigan: comparisons between ferry-based observations, shoreline-based DOAS observations and
527 model forecasts, *Atmospheric Chemistry and Physics*, 15, 5109-5122, 10.5194/acp-15-5109-2015,
528 2015.

529 Cleary, P. A., Dickens, A. J., McIlquham, M., Sanchez, M., Geib, K., Hedberg, C., Hupy, J., Watson,
530 M. W., Fuoco, M., Olson, E. R., Pierce, R. B., Stanier, C., Long, R., Valin, L., Conley, S., and Smith,
531 M.: Impacts of lake breeze meteorology on ozone gradient observations along Lake Michigan
532 Shorelines in Wisconsin, *Atmospheric Environment*, 269,
533 <https://doi.org/10.1016/j.atmosenv.2021.118834>, 2022b.

534 Cook, D. E., Strong, P. A., Garrett, S. A., and Marshall, R. E.: A small unmanned aerial system (UAS)
535 for coastal atmospheric research: preliminary results from New Zealand, *Journal of the Royal Society of*
536 *New Zealand*, 43, 108-115, 10.1080/03036758.2012.695280, 2013.

537 Crawford, T. L., Dobosy, R. J., McMillen, R. T., Vogel, C. A., and Hicks, B. B.: Air-surface exchange
538 measurement in heterogeneous regions: Extending tower observations with spatial structure observed
539 from small aircraft, *Global Change Biology*, 2, 275-285, 10.1111/j.1365-2486.1996.tb00079.x, 1996.

540 Crosman, E. T., Jacques, A. A., and Horel, J. D.: A novel approach for monitoring vertical profiles of
541 boundary-layer pollutants: Utilizing routine news helicopter flights, *Atmos. Pollut. Res.*, 8, 828-835,
542 10.1016/j.apr.2017.01.013, 2017.

543 de Boer, G., Elston, J., Houston, A., Pillar-Little, E., Argrow, B., Bell, T., Chilson, P., Choate, C.,
544 Greene, B., Islam, A., Detweiler, C., Jacob, J., Natalie, V., Rhodes, M., Rico, D., Stachura, M., Lappin,
545 F., Whyte, S., and Wilson, M.: Evaluation and Intercomparison of Small Uncrewed Aircraft Systems
546 Used for Atmospheric Research, in preparation, *Journal of Atmospheric and Oceanic Technology*,
547 2021.

548 DeMuer, D., Heylen, R., VanLoey, M., and DeSadelaeer, G.: Photochemical ozone production in the
549 convective mixed layer, studied with a tethered balloon sounding system, *Journal of Geophysical*
550 *Research-Atmospheres*, 102, 15933-15947, 10.1029/97jd01211, 1997.

551 Desjardins, R. L., Macpherson, J. I., Neumann, H., Denhartog, G., and Schuepp, P. H.: FLUX
552 ESTIMATES OF LATENT AND SENSIBLE HEAT, CARBON-DIOXIDE, AND OZONE USING
553 AN AIRCRAFT-TOWER COMBINATION, *Atmospheric Environment*, 29, 3147-3158, 10.1016/1352-
554 2310(95)00007-1, 1995.

555 Doak, A. G., Christiansen, M. B., D.A., H., Bertram, T. H., Carmichael, G., Cleary, P., Czarnetzki, A.
556 C., Dickens, A. F., Janssen, M., Kenski, M., Millet, D. B., Novak, G., Pierce, B. R., Stone, E. A.,
557 Szykman, J., Vermeuel, M., Wagner, T. J., Valin, L., and Stanier, C. O.: Characterization of ground-
558 based atmospheric pollution and meteorology sampling stations during the Lake Michigan Ozone Study
559 2017, *Journal of the Air & Waste Management Association*,
560 <https://doi.org/10.1080/10962247.2021.1900000>, 2021.

561 Dowell, D. C., Alexander, C. R., James, E. P., Weygandt, S. S., Benjamin, S. G., Manikin, G. S., Blake,
562 B. T., Brown, J. M., Olson, J. B., Hu, M., Smirnova, T. G., Ladwig, T., Kenyon, J. S., Ahmadov, R.,
563 Turner, D. D., Duda, J. D., and Alcott, T. I.: The High-Resolution Rapid Refresh (HRRR): An Hourly
564 Updating Convection-Allowing Forecast Model. Part I: Motivation and System Description, *Weather*
565 *and Forecasting*, 37, 1371-1395, 10.1175/waf-d-21-0151.1, 2022.

566 Fuhrer, J.: Ozone impacts on vegetation, *Ozone-Science & Engineering*, 24, 69-74,
567 10.1080/01919510208901597, 2002.

568 Gaza, R. S.: Mesoscale meteorology and high ozone in the northeast United States, *Journal of Applied*
569 *Meteorology*, 37, 961-977, 10.1175/1520-0450(1998)037<0961:Mmahoi>2.0.Co;2, 1998.

570 Gong, W. M., Mickle, R. E., Bottenheim, J., Froude, F., Beauchamp, S., and Waugh, D.: Marine/coastal
571 boundary layer and vertical structure of ozone observed at a coastal site in Nova Scotia during the 1996
572 NARSTO-CE field campaign, *Atmospheric Environment*, 34, 4139-4154, 10.1016/s1352-
573 2310(00)00226-0, 2000.

574 Greatwood, C., Richardson, T. S., Freer, J., Thomas, R. M., MacKenzie, A. R., Brownlow, R., Lowry,
575 D., Fisher, R. E., and Nisbet, E. G.: Atmospheric Sampling on Ascension Island Using Multirotor
576 UAVs, *Sensors*, 17, 24, 10.3390/s17061189, 2017.

577 Greenberg, J. R., Guenther, A. B., and Turnipseed, A.: Tethered balloon-based soundings of ozone,
578 aerosols, and solar radiation near Mexico City during MIRAGE-MEX, *Atmospheric Environment*, 43,
579 2672-2677, 10.1016/j.atmosenv.2009.02.019, 2009.

580 Greene, B. R., Segales, A. R., Bell, T. M., Pillar-Little, E. A., and Chilson, P. B.: Environmental and
581 Sensor Integration Influences on Temperature Measurements by Rotary-Wing Unmanned Aircraft
582 Systems, *Sensors*, 19, 10.3390/s19061470, 2019.

583 Gronoff, G., Robinson, J., Berkoff, T., Swap, R., Farris, B., Schroeder, J., Halliday, H. S., Knepp, T.,
584 Spinei, E., Carrion, W., Adcock, E. E., Johns, Z., Allen, D., and Pippin, M.: A method for quantifying
585 near range point source induced O₃ titration events using Co-located Lidar and Pandora measurements,
586 *Atmospheric Environment*, 204, 43-52, 10.1016/j.atmosenv.2019.01.052, 2019.

587 Guimaras, P., Ye, J. H., Batista, C., Barbosa, R., Ribeiro, I., Medeiros, A., Zhao, T. N., Hwang, W. C.,
588 Hung, H. M., Souza, R., and Martin, S. T.: Vertical Profiles of Atmospheric Species Concentrations and

589 Nighttime Boundary Layer Structure in the Dry Season over an Urban Environment in Central Amazon
590 Collected by an Unmanned Aerial Vehicle, *Atmosphere*, 11, 10.3390/atmos11121371, 2020.

591 Hanna, S. R. and Chang, J. C.: Relations between meteorology and ozone in the Lake Michigan region,
592 *Journal of Applied Meteorology*, 34, 670-678, 10.1175/1520-0450(1995)034<0670:rbmaoi>2.0.co;2,
593 1995.

594 Hemingway, B. L., Frazier, A. E., Elbing, B. R., and Jacob, J. D.: Vertical Sampling Scales for
595 Atmospheric Boundary Layer Measurements from Small Unmanned Aircraft Systems (sUAS),
596 *Atmosphere*, 8, 18, 10.3390/atmos8090176, 2017.

597 Herman, J., Cede, A., Spinei, E., Mount, G., Tzortziou, M., and Abuhassan, N.: NO₂ column amounts
598 from ground-based Pandora and MFDOAS spectrometers using the direct-sun DOAS technique:
599 Intercomparisons and application to OMI validation, *Journal of Geophysical Research-Atmospheres*,
600 114, 10.1029/2009jd011848, 2009.

601 Horel, J., Crosman, E., Jacques, A., Blaylock, B., Arens, S., Long, A., Sohl, J., and Martin, R.: Summer
602 ozone concentrations in the vicinity of the Great Salt Lake, *Atmospheric Science Letters*, 17, 480-486,
603 10.1002/asl.680, 2016.

604 Inoue, J. and Sato, K.: Toward sustainable meteorological profiling in polar regions: Case studies using
605 an inexpensive UAS on measuring lower boundary layers with quality of radiosondes, *Environmental*
606 *Research*, 205, 10.1016/j.envres.2021.112468, 2022.

607 Jacob, J. D., Chilson, P. B., Houston, A. L., and Smith, S. W.: Considerations for Atmospheric
608 Measurements with Small Unmanned Aircraft Systems, *Atmosphere*, 9, 16, 10.3390/atmos9070252,
609 2018.

610 Kaser, L., Patton, E. G., Pfister, G. G., Weinheimer, A. J., Montzka, D. D., Flocke, F., Thompson, A.
611 M., Stauffer, R. M., and Halliday, H. S.: The effect of entrainment through atmospheric boundary layer
612 growth on observed and modeled surface ozone in the Colorado Front Range, *Journal of Geophysical*
613 *Research-Atmospheres*, 122, 6075-6093, 10.1002/2016jd026245, 2017.

614 Kim, J., Shusterman, A. A., Lieschke, K. J., Newman, C., and Cohen, R. C.: The BERkeley Atmospheric
615 CO₂ Observation Network: field calibration and evaluation of low-cost air quality sensors, *Atmospheric*
616 *Measurement Techniques*, 11, 1937-1946, 10.5194/amt-11-1937-2018, 2018.

617 Kimball, S. K., Montalvo, C. J., and Mulekar, M. S.: Evaluating Temperature Measurements of the
618 iMET-XQ, in the Field, under Varying Atmospheric Conditions, *Atmosphere*, 11,
619 10.3390/atmos11040335, 2020.

620 Knapp, K. G., Jensen, M. L., Balsley, B. B., Bognar, J. A., Oltmans, S. J., Smith, T. W., and Birks, J.
621 W.: Vertical profiling using a complementary kite and tethered balloon platform at Ferryland Downs,
622 Newfoundland, Canada: Observation of a dry, ozone-rich plume in the free troposphere, *Journal of*
623 *Geophysical Research-Atmospheres*, 103, 13389-13397, 10.1029/97jd01831, 1998.

624 Koch, S. E., Fengler, M., Chilson, P. B., Elmore, K. L., Argrow, B., Andra, D. L., and Lindley, T.: On
625 the Use of Unmanned Aircraft for Sampling Mesoscale Phenomena in the Preconvective Boundary
626 Layer, *Journal of Atmospheric and Oceanic Technology*, 35, 2265-2288, 10.1175/jtech-d-18-0101.1,
627 2018.

628 Krechmer, J., Lopez-Hilfiker, F., Koss, A., Hutterli, M., Stoermer, C., Deming, B., Kimmel, J.,
629 Warneke, C., Holzinger, R., Jayne, J., Worsnop, D., Fuhrer, K., Gonin, M., and de Gouw, J.: Evaluation

630 of a New Reagent-Ion Source and Focusing Ion-Molecule Reactor for Use in Proton-Transfer-Reaction
631 Mass Spectrometry, *Analytical Chemistry*, 90, 12011-12018, 10.1021/acs.analchem.8b02641, 2018.

632 Levy, I., Makar, P. A., Sills, D., Zhang, J., Hayden, K. L., Mihele, C., Narayan, J., Moran, M. D.,
633 Sjostedt, S., and Brook, J.: Unraveling the complex local-scale flows influencing ozone patterns in the
634 southern Great Lakes of North America, *Atmospheric Chemistry and Physics*, 10, 10895-10915,
635 10.5194/acp-10-10895-2010, 2010.

636 Li, X. B., Peng, Z. R., Lu, Q. C., Wang, D. F., Hu, X. M., Wang, D. S., Li, B., Fu, Q. Y., Xiu, G. L., and
637 He, H. D.: Evaluation of unmanned aerial system in measuring lower tropospheric ozone and fine
638 aerosol particles using portable monitors, *Atmospheric Environment*, 222,
639 10.1016/j.atmosenv.2019.117134, 2020.

640 Li, X. B., Wang, D. F., Lu, Q. C., Peng, Z. R., Fu, Q. Y., Hu, X. M., Huo, J. T., Xiu, G. L., Li, B., Li,
641 C., Wang, D. S., and Wang, H. Y.: Three-dimensional analysis of ozone and PM_{2.5} distributions
642 obtained by observations of tethered balloon and unmanned aerial vehicle in Shanghai, China, *Stoch.*
643 *Environ. Res. Risk Assess.*, 32, 1189-1203, 10.1007/s00477-018-1524-2, 2018.

644 Li, Y. W., Liu, B., Ye, J. H., Jia, T. J., Khuzestani, R. B., Jia, Y. S., Cheng, X., Zheng, Y., Li, X., Wu,
645 C., Xin, J. Y., Wu, Z. H., Tomoto, M. A., McKinney, K. A., Martin, S. T., Yong, J. L., and Chen, Q.:
646 Unmanned Aerial Vehicle Measurements of Volatile Organic Compounds over a Subtropical Forest in
647 China and Implications for Emission Heterogeneity, *Acs Earth and Space Chemistry*, 5, 247-256,
648 10.1021/acsearthspacechem.0c00271, 2021.

649 Lu, R. and Turco, R. P.: AIR POLLUTANT TRANSPORT IN A COASTAL ENVIRONMENT .1. 2-
650 DIMENSIONAL SIMULATIONS OF SEA-BREEZE AND MOUNTAIN EFFECTS, *Journal of the*
651 *Atmospheric Sciences*, 51, 2285-2308, 10.1175/1520-0469(1994)051<2285:Aptiac>2.0.Co;2, 1994.

652 Lyman, S. and Tran, T.: Inversion structure and winter ozone distribution in the Uintah Basin, Utah,
653 USA, *Atmospheric Environment*, 123, 156-165, 10.1016/j.atmosenv.2015.10.067, 2015.

654 Mazzuca, G. M., Pickering, K. E., Clark, R. D., Loughner, C. P., Fried, A., Zweers, D. C. S.,
655 Weinheimer, A. J., and Dickerson, R. R.: Use of tethered sonde and aircraft profiles to study the impact of
656 mesoscale and microscale meteorology on air quality, *Atmospheric Environment*, 149, 55-69,
657 10.1016/j.atmosenv.2016.10.025, 2017.

658 McNider, R. T., Pour-Biazar, A., Doty, K., White, A., Wu, Y. L., Qin, M. M., Hu, Y. T., Odman, T.,
659 Cleary, P., Knipping, E., Dornblaser, B., Lee, P., Hain, C., and McKeen, S.: Examination of the
660 Physical Atmosphere in the Great Lakes Region and Its Potential Impact on Air Quality Overwater
661 Stability and Satellite Assimilation, *Journal of Applied Meteorology and Climatology*, 57, 2789-2816,
662 10.1175/jamc-d-17-0355.1, 2018.

663 Novak, G. A., Vermeuel, M. P., and Bertram, T. H.: Simultaneous detection of ozone and nitrogen
664 dioxide by oxygen anion chemical ionization mass spectrometry: a fast-time-response sensor suitable
665 for eddy covariance measurements, *Atmospheric Measurement Techniques*, 13, 1887-1907,
666 10.5194/amt-13-1887-2020, 2020.

667 Ollison, W. M., Crow, W., and Spicer, C. W.: Field testing of new-technology ambient air ozone
668 monitors, *Journal of the Air & Waste Management Association*, 63, 855-863,
669 10.1080/10962247.2013.796898, 2013.

670 Peng, Y. P., Chen, K. S., Lou, J. C., Hwang, S. W., Wang, W. C., Lai, C. H., and Tsai, M. Y.:
671 Measurements and Mesoscale Modeling of Autumnal Vertical Ozone Profiles in Southern Taiwan,
672 *Terrestrial Atmospheric and Oceanic Sciences*, 19, 505-514, 10.3319/tao.2008.19.5.505(a), 2008.
673 Sillman, S.: The relation between ozone, NO_x and hydrocarbons in urban and polluted rural
674 environments, *Atmospheric Environment*, 33, 1821-1845, 10.1016/s1352-2310(98)00345-8, 1999.
675 Sills, D. M. L., Brook, J. R., Levy, I., Makar, P. A., Zhang, J., and Taylor, P. A.: Lake breezes in the
676 southern Great Lakes region and their influence during BAQS-Met 2007, *Atmospheric Chemistry and*
677 *Physics*, 11, 7955-7973, 10.5194/acp-11-7955-2011, 2011.
678 Stanier, C. O., Pierce, R. B., Abdi-Oskouei, M., Adelman, Z. E., Al-Saadi, J., Alwe, H. D., Bertram, T.
679 H., Carmichael, G. R., Christiansen, M. B., Cleary, P. A., Czarnetzki, A. C., Dickens, A. F., Fuoco, M.
680 A., Hughes, D. D., Hupy, J. P., Janz, S. J., Judd, L. M., Kenski, D., Kowalewski, M. G., Long, R. W.,
681 Millet, D. B., Novak, G., Roozitalab, B., Shaw, S. L., Stone, E. A., Szykman, J., Valin, L., Vermeuel,
682 M., Wagner, T. J., Whitehill, A. R., and Williams, D. J.: Overview of the Lake Michigan Ozone Study
683 2017, *Bulletin of the American Meteorological Society*, 102, E2207-E2225, 10.1175/bams-d-20-0061.1,
684 2021.
685 Sullivan, J. T., Berkoff, T., Gronoff, G., Knepp, T., Pippin, M., Allen, D., Twigg, L., Swap, R.,
686 Tzortziou, M., Thompson, A. M., Stauffer, R. M., Wolfe, G. M., Flynn, J., Pusede, S. E., Judd, L. M.,
687 Moore, W., Baker, B. D., Al-Saadi, J., and McGee, T. J.: The Ozone Water-Land Environmental
688 Transition Study: An Innovative Strategy for Understanding Chesapeake Bay Pollution Events, *Bulletin*
689 *of the American Meteorological Society*, 100, 291-306, 10.1175/bams-d-18-0025.1, 2019.
690 Sun, J. L., Desjardins, R., Mahrt, L., and MacPherson, I.: Transport of carbon dioxide, water vapor, and
691 ozone by turbulence and local circulations, *Journal of Geophysical Research-Atmospheres*, 103, 25873-
692 25885, 10.1029/98jd02439, 1998.
693 Tang, G. Q., Liu, Y. T., Huang, X., Wang, Y. H., Hu, B., Zhang, Y. C., Song, T., Li, X. L., Wu, S., Li,
694 Q. H., Kang, Y. Y., Zhu, Z. Y., Wang, M., Wang, Y. M., Li, T. T., Li, X., and Wang, Y. S.: Aggravated
695 ozone pollution in the strong free convection boundary layer, *Science of the Total Environment*, 788,
696 10.1016/j.scitotenv.2021.147740, 2021.
697 Tang, Y. H., Lee, P., Tsidulko, M., Huang, H. C., McQueen, J. T., DiMego, G. J., Emmons, L. K.,
698 Pierce, R. B., Thompson, A. M., Lin, H. M., Kang, D. W., Tong, D., Yu, S. C., Mathur, R., Pleim, J. E.,
699 Otte, T. L., Pouliot, G., Young, J. O., Schere, K. L., Davidson, P. M., and Stajner, I.: The impact of
700 chemical lateral boundary conditions on CMAQ predictions of tropospheric ozone over the continental
701 United States, *Environmental Fluid Mechanics*, 9, 43-58, 10.1007/s10652-008-9092-5, 2009.
702 Tanimoto, H., Zbinden, R. M., Thouret, V., and Nedelec, P.: Consistency of tropospheric ozone
703 observations made by different platforms and techniques in the global databases, *Tellus Series B-*
704 *Chemical and Physical Meteorology*, 67, 10.3402/tellusb.v67.27073, 2015.
705 Tarasick, D., Galbally, I. E., Cooper, O. R., Schultz, M. G., Ancellet, G., Leblanc, T., Wallington, T. J.,
706 Ziemke, J., Liu, X., Steinbacher, M., Staehelin, J., Vigouroux, C., Hannigan, J. W., Garcia, O., Foret,
707 G., Zanis, P., Weatherhead, E., Petropavlovskikh, I., Worden, H., Osman, M., Liu, J., Chang, K. L.,
708 Gaudel, A., Lin, M. Y., Granados-Munoz, M., Thompson, A. M., Oltmans, S. J., Cuesta, J., Dufour, G.,
709 Thouret, V., Hassler, B., Trickl, T., and Neu, J. L.: Tropospheric Ozone Assessment Report:
710 Tropospheric ozone from 1877 to 2016, observed levels, trends and uncertainties, *Elementa-Science of*
711 *the Anthropocene*, 7, 10.1525/elementa.376, 2019.

712 Telg, H., Murphy, D. M., Bates, T. S., Johnson, J. E., Quinn, P. K., Giardi, F., and Gao, R. S.: A
713 practical set of miniaturized instruments for vertical profiling of aerosol physical properties, *Aerosol*
714 *Sci. Technol.*, 51, 715-723, 10.1080/02786826.2017.1296103, 2017.

715 Tirado, J., Torti, A. O., Butterworth, B. J., Wangen, K., Voon, A., Kies, B., Hupy, J. P., de Boer, G.,
716 Pierce, R. B., Wagner, T. J., and Cleary, P. A.: Observations of coastal dynamics during lake breeze at a
717 shoreline impacted by high ozone, DOI: 10.1039/D2EA00101B 2023.

718 Verhoelst, T., Compernelle, S., Pinardi, G., Lambert, J. C., Eskes, H. J., Eichmann, K. U., Fjaeraa, A.
719 M., Granville, J., Niemeijer, S., Cede, A., Tiefengraber, M., Hendrick, F., Pazmino, A., Bais, A.,
720 Bazureau, A., Boersma, K. F., Bogner, K., Dehn, A., Donner, S., Elokhov, A., Gebetsberger, M.,
721 Goutail, F., de la Mora, M. G., Gruzdev, A., Gratsea, M., Hansen, G. H., Irie, H., Jepsen, N., Kanaya,
722 Y., Karagiozidis, D., Kivi, R., Kreher, K., Levelt, P. F., Liu, C., Muller, M., Comas, M. N., PETERS, A.
723 J. M., Pommereau, J. P., Portafaix, T., Prados-Roman, C., Puentedura, O., Querel, R., Remmers, J.,
724 Richter, A., Rimmer, J., Cardenas, C. R., de Miguel, L. S., Sinyakov, V. P., Stremme, W., Strong, K.,
725 Van Roozendaal, M., Veefkind, J. P., Wagner, T., Wittrock, F., Gonzalez, M. Y., and Zehner, C.:
726 Ground-based validation of the Copernicus Sentinel-5P TROPOMI NO₂ measurements with the
727 NDACC ZSL-DOAS, MAX-DOAS and Pandonia global networks, *Atmospheric Measurement*
728 *Techniques*, 14, 481-510, 10.5194/amt-14-481-2021, 2021.

729 Vermeuel, M. P., Cleary, P. A., Desai, A. R., and Bertram, T. H.: Simultaneous Measurements of O-3
730 and HCOOH Vertical Fluxes Indicate Rapid In-Canopy Terpene Chemistry Enhances O-3 Removal
731 Over Mixed Temperate Forests, *Geophysical Research Letters*, 48, 10.1029/2020gl090996, 2021.

732 Vermeuel, M. P., Novak, G. A., Kilgour, D. B., Clafin, M. S., Lerner, B. M., Trowbridge, A. M., Thom,
733 J., Cleary, P. A., Desai, A. R., and Bertram, T. H.: Observations of biogenic volatile organic compounds
734 over a mixed temperate forest during the summer to autumn transition, *Atmospheric Chemistry and*
735 *Physics*, 23, 4123–4148, <https://doi.org/10.5194/acp-23-4123-2023>, 2023.

736 Vermeuel, M. P., Novak, G. A., Alwe, H. D., Hughes, D. D., Kaleel, R., Dickens, A. F., Kenski, D.,
737 Czarnetzki, A. C., Stone, E. A., Stanier, C. O., Pierce, R. B., Millet, D. B., and Bertram, T. H.:
738 Sensitivity of Ozone Production to NO_x and VOC Along the Lake Michigan Coastline, *Journal of*
739 *Geophysical Research-Atmospheres*, 124, 10989-11006, 10.1029/2019jd030842, 2019.

740 Wagner, T. J., Czarnetzki, A. C., Christiansen, M., Pierce, R. B., Stanier, C. O., Dickens, A. F., and
741 Eloranta, E. W.: Observations of the Development and Vertical Structure of the Lake Breeze
742 Circulation During the 2017 Lake Michigan Ozone Study, *Journal of the Atmospheric Sciences*, 79,
743 1005-1020, <https://doi.org/10.1175/JAS-D-20-0297.1>, 2022.

744 Wainwright, C. E., Bonin, T. A., Chilson, P. B., Gibbs, J. A., Fedorovich, E., and Palmer, R. D.:
745 Methods for Evaluating the Temperature Structure-Function Parameter Using Unmanned Aerial
746 Systems and Large-Eddy Simulation, *Boundary-Layer Meteorology*, 155, 189-208, 10.1007/s10546-
747 014-0001-9, 2015.

748 Wilson, K. L. and Birks, J. W.: Mechanism and elimination of a water vapor interference in the
749 measurement of ozone by UV absorbance, *Environmental Science & Technology*, 40, 6361-6367,
750 10.1021/es052590c, 2006.

751 Witte, J. C., Thompson, A. M., Smit, H. G. J., Vomel, H., Posny, F., and Stubi, R.: First Reprocessing
752 of Southern Hemisphere ADDitional OZonesondes Profile Records: 3. Uncertainty in Ozone Profile and

753 Total Column, *Journal of Geophysical Research-Atmospheres*, 123, 3243-3268, 10.1002/2017jd027791,
754 2018.

755 Wu, C., Liu, B., Wu, D., Yang, H. L., Mao, X., Tan, J., Liang, Y., Sun, J. Y., Xia, R., Sun, J. R., He, G.
756 W., Li, M., Deng, T., Zhou, Z., and Li, Y. J.: Vertical profiling of black carbon and ozone using a
757 multicopter unmanned aerial vehicle (UAV) in urban Shenzhen of South China, *Science of the Total*
758 *Environment*, 801, 10.1016/j.scitotenv.2021.149689, 2021.

759 Wu, Y. L., Lin, C. H., Lai, C. H., Lai, H. C., and Young, C. Y.: Effects of Local Circulations, Turbulent
760 Internal Boundary Layers, and Elevated Industrial Plumes on Coastal Ozone Pollution in the Downwind
761 Kaohsiung Urban-Industrial Complex, *Terrestrial Atmospheric and Oceanic Sciences*, 21, 343-357,
762 10.3319/tao.2009.04.14.01(a), 2010.

763 Xu, Z. N., Huang, X., Nie, W., Shen, Y. C., Zheng, L. F., Xie, Y. N., Wang, T. Y., Ding, K., Liu, L. X.,
764 Zhou, D. R., Qi, X. M., and Ding, A. J.: Impact of Biomass Burning and Vertical Mixing of Residual-
765 Layer Aged Plumes on Ozone in the Yangtze River Delta, China: A Tethered-Balloon Measurement
766 and Modeling Study of a Multiday Ozone Episode, *Journal of Geophysical Research-Atmospheres*, 123,
767 11786-11803, 10.1029/2018jd028994, 2018.

768 Ye, J., Batista, C. E., Zhao, T., Campos, J., Ma, Y., Guimarães, P., Ribeiro, I. O., Medeiros, A. S. S.,
769 Stewart, M. P., Vilà-Guerau de Arellano, J., Guenther, A. B., Souza, R. A. F. d., and Martin, S. T.:
770 River Winds and Transport of Forest Volatiles in the Amazonian Riparian Ecoregion, *Environmental*
771 *Science & Technology*, 56, 12667-12677, 10.1021/acs.est.1c08460, 2022.

772 Zhang, J., Ninneman, M., Joseph, E., Schwab, M. J., Shrestha, B., and Schwab, J. J.: Mobile Laboratory
773 Measurements of High Surface Ozone Levels and Spatial Heterogeneity During LISTOS 2018:
774 Evidence for Sea Breeze Influence, *Journal of Geophysical Research-Atmospheres*, 125,
775 10.1029/2019jd031961, 2020.

776 Zhang, K., Zhou, L., Fu, Q. Y., Yan, L., Bian, Q. G., Wang, D. F., and Xiu, G. L.: Vertical distribution
777 of ozone over Shanghai during late spring: A balloon-borne observation, *Atmospheric Environment*,
778 208, 48-60, 10.1016/j.atmosenv.2019.03.011, 2019.

779